Few Layer Graphene/TiO 2 Composites for Enhanced Solar-Driven H 2 Production from Methanol

Hamza El Marouazi, Pablo Jiménez-Calvo, Edouard Breniaux, Christophe Colbeau-Justin, Izabela Janowska, Valérie Keller

Few Layer Graphene/TiO_2 composites for enhanced solar-driven H_2 production from methanol.

Hamza El Marouazi [†], Pablo Jiménez-Calvo [†], Edouard Breniaux,[†] Christophe Colbeau-Justin[‡], Izabela Janowska [†*], Valerie Keller [†*]

[†] Institut de Chimie et des Procédés pour l'Énergie, l'Environnement et la Santé, CNRS/Université de Strasbourg, 25, rue Becquerel 67087 Strasbourg Cedex 2, France

[‡] Institut de Chimie Physique, CNRS UMR 8000, Université Paris-Saclay, Bâtiment 349, 91405 Orsay Cedex, France

* Corresponding authors: janowskai@unistra.fr, tel. +33 68852633

vkeller@unistra.fr, tel. +33 68852736

Here is presented the elaboration of Few Layer Graphene/TiO_2 photocatalytic composites (FLG/TiO_2) with FLG loadings from 0.5 to 11 wt.%. Contrary to commonly used (reduced) graphene oxide obtained by long and harsh conditions synthesis, FLG was synthesized by simple, fast, efficient and eco-friendly exfoliation method. The enhancement of defective/functionalized sites density for attachment of TiO_2 species was achieved via calcination process at 450 °C. The nanocomposites were evaluated toward H_2 production from methanol under artificial solar light irradiation, without the use of a co-catalyst. It was observed that the best activities are provided by the composites with the lowest loading: 0.5 and 1.0 wt.% FLG/TiO_2 that are 2-3 times more efficient than reference and commercial TiO_2. The photocatalytic activity of the composites was correlated to their surface area, morphological, structural, optical properties and kinetics of free electron mobility properties. The enhanced activity is attributed to higher surface area, better photogenerated charges separation thanks to electrons' delocalization and trapping onto graphene layers well interfaced with TiO_2 nanoparticles, but also to additional FLG visible light absorption properties and charge carriers' generation. The impact of enhanced FLG edges defects/functionalities is reflected as well via selected analysis and hydrogen generation.

Keywords: Few Layer Graphene (FLG); graphene-TiO_2 composite; H_2 production; methanol photoreforming; graphene edges defects, TRMC

Introduction

Within a large number of studies dealing with photocatalysis for environmental or energy applications, TiO_2 is one of the most efficient and thus widely studied semiconductor [1-3]. However, it suffers amongst other drawbacks from its wide band-gap allowing to use only less than 4% (UV part) of the total incident solar spectrum [4]. Recently, the research strategy of TiO_2-based photocatalysis (as for other semiconductors (SCs)) is focused on rational design and engineering of hybrid systems.[5, 6] TiO_2 association at its nanometric interface with other narrow band gap SCs aims at simultaneously enhancing visible light activation, reducing electron-hole recombination rate and increasing adsorption capacity. Following the heterostructure formation approach, modification of TiO_2 with carbonaceous nanomaterials (carbon nanotubes, fullerenes, graphene, …) has attracted increased attention [7-10]. In particular, combination of TiO_2 with graphene might be considered as a promising strategy for enhancing solar-light driven photocatalytic performance [11-13]. One of the most important characteristics of graphene for photocatalysis is its ability to tune the band gap energy of semiconductors. In addition, the presence of graphene, due to its high electron mobility, contributes to the suppression of the rapid recombination of electron–hole pairs, thus leading to an enhancement in photocatalytic activity [14-18]. Furthermore, graphene shows exceptional adsorption ability toward various classes of compounds promoting their adsorption, prerequisite for their efficient photocatalytic activity. The methods for the graphene preparation are numerous [19-21] but generally the synthesis of non-functionalized graphene does not allow the production of TiO_2-graphene hybrid materials due to the absence of functional groups able to bond to the semiconductor [22-23].

Graphene-based nanocomposites preparation for photocatalytic purposes [18, 24] are prepared by anchoring semiconductor nanostructures onto graphene using three main strategies [18, 24]. One of the most popular methodology involves graphene oxide (GO) showing a high density of oxygen functional groups. The method allows two approaches, the formation of photocatalytic nanoparticles directly on GO surface using the oxygen-containing groups as nucleation sites for the nanoparticle growth or the adhesion of the photocatalysts onto GO through sonication or stirring [14, 24, 25]. Despite this facility of TiO_2 attachment, a drawback of GO is related to its long and harsh synthesis as well as necessity of its reduction in order to

restore conjugated sp^2- carbon lattice. Usually GO can be reduced only partially, till now by thermal [26], chemical [27], electrochemical [28], microwave [29], sonochemical [30] or photocatalytic methods [31]. Hydrothermal/solvothermal methods have also been studied using one-pot synthesis allowing the additional advantage of reducing GO during the formation process of TiO_2 [26, 32]. However, even if reduction of GO removes a large amount of its oxygen, complete reduction remains still challenging to reach the mechanical and electronic properties of graphene [33,34] and the final material is defined as reduced GO (rGO) [35, 36]. The preparation of graphene-TiO_2 photocatalytic composites starting from graphene sheets is scarce and highly challenging so far [37]. A possible use of other type of graphene such as FLG which can be obtained by simple, faster and commercially valuable method in the field of photocatalysis is almost non-existed. Challenging is indeed with FLG to avoid the excessive absorption of in-put photons making a screening effect as well as appropriate attachment of TiO_2 species due to the low amount of surface defects.

Herein we report for the first time the synthesis of FLG-TiO_2 composites with different FLG loading, where stable FLG flakes dispersions are first obtained via rapid, efficient, simple and environmentally friendly method *i.e*. from exfoliation of graphite in water using Bovine Serum Albumin (BSA) as exfoliating bio-surfactant. The sufficient amount of defective sites on FLG to stabilized and produce good interface with TiO_2 species was achieved via calcination process and additionally by prolonged exfoliation of graphite. The photocatalytic activity of the composites toward solar light driven H_2 production from methanol photoreforming are investigated together with scrupulous determination of their physico-chemical characterization and properties.

Experimental Section

Preparation of the photocatalysts

FLG material was synthetized following an optimized method [38] starting from expanded graphite (EG, from Carbon Lorraine), and Bovine Serum Albumin (BSA, Sigma Aldrich, purity > 98%) in water. EG, BSA and distilled water with a ratio of 10:1:5, respectively, were ultrasonicated with a tip sonicator at 80 W for 2 h. After a sedimentation of 2 h, the separated stable colloid, with a concentration of around 1.75 g/l, was dried at 100 °C for 24 h and the resulting powder of FLG covered by BSA was recuperated to use it after.
Alternatively, the ultrasonication of EG was performed during 5 h at 160 W (FLG').

The FLG/TiO_2 (and FLG'/TiO_2) nanocomposites were synthesized in two steps. First, the dried FLG (or FLG') was dispersed in ethanol and sonicated for 40 min (sonication bath, 280 W), and the stable phase was recuperated after 3 h of decantation. In a second step, a sol-gel method previously reported for TiO_2 synthesis was applied [39]: Tetraisopropylorthotitanate ($Ti(OC_3H_7)_4$, TIP) was added to the previously dispersed FLG in ethanol with different concentration (CARLO ERBA Reagents, 99.9%). After 30 min of stirring, acetic acid (Prolabo, 99.5%) mixed with distilled water was drop wise added to form a sol considering the molar ratio: TIP/acetic acid /ethanol/water of 1/18.60/18.36/0.82. The resulting precursor solution was stirred at room temperature for 1h and then kept in the dark for 24 h for gellification. Finally, the gel was dried at 100 °C for 24 h and then calcined for 3 h under air at 450 °C (heating ramp of 5 °C/min). The obtained FLG (FLG')/TiO_2 composites had a FLG (FLG') loadings varying from 0.5 to 11 wt.%. In total, nine composites were prepared: five containing FLG (0.5% FLG/TiO_2, 1% FLG/TiO_2, 1.5% FLG/TiO_2, 4.5% FLG/TiO_2, 11% FLG/TiO_2) and four containing FLG'(0.5% FLG'/TiO_2, 2% FLG'/TiO_2, 2.5% FLG'/TiO_2, 3.5% FLG'/TiO_2).

The values of FLG (FLG') content in the composites were obtained via TGA analysis, and round to the nearest half unit (0.5).

For comparison, bare TiO_2 NPs (TiO_2 SG) was synthesized by the same sol-gel procedure (without addition of FLG or FLG').

Two commercially available TiO_2 samples, TiO_2 P25 (Evonik, 75% anatase/25% rutile) and TiO_2 UV 100 (Sachtleben, 100% anatase) were also used for comparison purposes.

Characterization methods

Thermogravimetric analyses (TGA) were performed using a TA Instrument Q5000IR. Each sample was placed in a platinum crucible and heated from room temperature up to 1000 °C with a heating rate of 10 °C.min^{-1} under air flow of 25 mL.min^{-1}. Standard deviation on the decomposition temperature of the as-prepared samples is ± 10 °C.

Near Infra-Red (NIR) Raman spectra were recorded with a LabRAM ARAMIS Horiba Raman spectrometer equipped with a Synapse CCD Detector, an Olympus BX41 Microscope and a 532 nm laser excitation (Laser Quantum MPC600 PSU).

Nitrogen adsorption-desorption isotherm measurements were conducted at liquid N_2 temperature using a Micromeritics Asap 2420 porosimeter. Before the N_2 adsorption, the samples were outgassed at 150 °C overnight to desorb the impurities or moisture from its

surfaces. Specific surface areas were calculated by the Brunauer, Emmett and Teller (BET) method in the relative pressure (p/p_0) range 0.05-0.3 and using t-plots methods. Pore-size distributions were calculated by the Barret-Joyner-Halenda (BJH) method, which is specific for mesoporous solids.

X-ray photoelectron spectroscopy (XPS) analyses were performed in a Thermo-VG scientific spectrometer equipped with a CLAM4 (MCD) hemispherical electron analyzer. The Al Kα line (1486.6 eV) of a dual anode X-ray source was used as incident radiation. High resolution spectra were recorded in constant pass energy mode (20 eV). The energy shift due to electrostatic charging was subtracted using the carbon adventitious signal *i.e.* the C 1s peak located at 284.6 eV or Ti at 458.401 eV. Surface atomic ratios were derived from XPS spectra using a Shirley-type background considering the appropriate experimental sensitivity factors of the normalized photo ionization cross-section of the atomic subshells as determined by Scofield [40]. UPS analyses (hν = 21.2 eV) were performed by applying a bias of 15.32 V to the sample to avoid interference of the spectrometer threshold in the UP spectra. The values of the VBM were determined by fitting a straight line onto the leading edge.

High Resolution Transmission Electron Microscopy (HRTEM) was performed on a JEOL 2100F LaB_6 TEM/STEM microscope operating at 200 kV and with a point-to-point resolution of 0.21 nm. The sample was sonicated in ethanol before a drop of the suspension was deposited onto the microscopic TEM grid.

Composition and crystallinity of the samples were characterized by X-ray powder diffraction (XRD) on a D8 Advance Bruker diffractometer using Cu-kα radiation (λ=1.5406 Å). The data were acquired in step scan mode over the 2θ range 20–80°, using a step interval of 0.02° and a counting time of 1 s per step. Average TiO_2 anatase mean crystallite size was determined using the Debye-Scherrer equation based on the full width at half-maximum and the position of the (101) main reflection.

The optical properties of the samples were determined via a UV-Vis diffuse reflectance spectrophotometer (Perkin Elmer Lambda 950 Scan) equipped with diffuse reflectance integrating sphere.

The charge-carrier lifetimes in the samples after laser pulses at 360 nm and 450 nm were determined by microwave absorption experiments using the Time Resolved Microwave Conductivity method (TRMC) [41]. The TRMC technique is based on the measurement of the

change of the microwave power reflected by a sample, $\Delta P(t)$, induced by its laser pulsed illumination. The incident microwaves were generated by a Gunn diode of the K_α band at 30 GHz. Pulsed light source was an OPO laser (EKSPLA, NT342B) tunable from 225 to 2000 nm. It delivers 8 ns fwmh pulses with a frequency of 10 Hz. The light energy densities received by the sample were 1.3 and 2.2 mJ.cm^{-2} at 360 and 450 nm, respectively. The main data provided by TRMC are the maximum value of the signal (I_{max}), which indicates the number of the excess charge carriers created by the pulse, including decay processes during the excitation by the laser (10 ns), and the decay (I(t)) due to the decrease of the excess electrons, either by recombination or trapping processes. Comparing I_{max}/I_{40ns} is considered as being relevant to get information about the kinetics of free electrons mobility [42].

Procedures of the photocatalytic tests

The production of H_2 was carried out in a quartz vessel containing 900 ml of methanol (assay (GLC)>99.9%) in ultrapure water at a concentration of 17.3 mol/l. The setup is equipped with a jacket quartz tube containing 150 W Ceramic-Metal-Halide Hg Lamp, simulating the artificial solar light (31.9 mW.cm^{-2}), containing 7.8% of UV wavelengths from 280-400 nm. The corresponding emission spectrum is given in Fig. S1 (see Supporting Information). The photocatalytic tests were carried out with the photocatalytic materials dispersed in methanol (after sonication at 20 W for 2 min). Two different concentrations, 0.1 and 0.2 g/L, were tested with a mechanical stirring at 700 rpm and under 100 mL.min^{-1} nitrogen flow. Before starting the photocatalytic experiences, the reactor was sealed and flushed with nitrogen for 1h in order to remove residual oxygen. The temperature of the suspension was kept at 25 °C by an external cooling jacket with recycled water. The concentration of H_2 was measured with a micro-gas chromatograph (SRA Instruments R-3000) equipped with a thermal conductivity detector (TCD).

Quantum yield (QY) values were determined using equation 1, where $\boldsymbol{r_{(m)H_2}}$ is defined as the hydrogen formation rate (mol.h^{-1}) considering the overall methanol photoreforming reaction and $\boldsymbol{q_p}$ is defined as the photon flux of the lamp and is equal to 0.43 mol.h^{-1}. 3 is the number of H_2 molecules produced from one photon.

To determine the photon flux, the absolute irradiance of the lamp (from 300 to 800 nm) was measured using an ILT900-R spectroradiometer (International Light Technologies).

$$\boldsymbol{QY}\ (\%) = \mathbf{3} \times \frac{\boldsymbol{r_{(m)_{H2}}}}{\boldsymbol{q_p}} \times \mathbf{100} \qquad \textbf{(1)}$$

Results and Discussion

Investigation of materials

The detailed investigations showed below concerns mostly the composites containing FLG obtained after 2h of exfoliation of EG with FLG loadings from 0.5 to 11 wt.% (0.5% FLG/TiO_2, 1% FLG/TiO_2, 1.5% FLG/TiO_2, 4.5% FLG/TiO_2, 11% FLG/TiO_2). As detailed in the experimental part, the formation of the composites is carried out via sol-gel method followed by calcination step at 450 °C. In order however to check the effect of defects amount in FLG on the formation of interface with TiO_2 species, *i.e.* on the optimum minimum loading of FLG efficient in hydrogen production, the exfoliation of EG was also performed during 5 h at 160 W (FLG') and four composites containing FLG' were prepared. It was indeed previously reported that prolonged duration of such ultrasonication- assisted exfoliation in water leads to enhanced defects content that is mostly related to enhanced number of FLG edges via the excessive cutting of FLG flakes [38]. The one efficient composite containing the smallest amount of FLG' (0.5% FLG'/TiO_2) is studied and presented below, while more details concerning the three other FLG' composites as well as the results of hydrogen production tests for all FLG' containing composites are additionally showed in SI. TGA profile of FLG sample (Fig. 1-inset) exhibits a first weight loss at 250 °C that can be assigned to BSA oxidation, followed by the second and major loss at 550 °C due to the carbon oxidation. The combustion curves are shifted towards lower temperatures in FLG' compared to FLG, and e.g. the temperature corresponding to 50% of weight loss is shifted by 40 °C. This shift confirms higher amount of defects in the sample. From TGA analysis of the FLG/TiO_2 composites with various FLG contents (Fig. 1), one can observe three main domains of weight loss. The first contribution until *ca.* 200 °C, is attributed to water and adsorbates desorption, a second one between 200 and approximately 450 °C exhibiting small weight loss due to TiO_2 dehydroxylation and a third one at approximately 550 °C related to carbon burning. This last contribution was used to calculate the FLG content (wt.%). When comparing the TGA profile related to FLG calcinated at 450 °C (inset) and the one of BSA, one can assume that in our calcination conditions (at 450 °C for 3 h), *quasi* no more BSA is remaining in the composite materials. The 40% of BSA remaining at

450 °C in TGA curve represents less than 1% in the composite with the highest FLG loading, while its real amount is even lower taking into account that duration of calcination treatment at 450 °C is much longer than duration of TGA analysis at this temperature.

The impact of calcination process on FLG defects content can be observed by the maximum % of FLG' that can be obtained in the composites comparing to the FLG containing composites. In other words, the same initial amount and ratio of carbon during the preparation of the composites, after calcination, decreases in more significant manner. Consequently, the composites: 0.5% FLG'/TiO_2, 2 %FLG'/TiO_2, 2.5% FLG'/TiO_2, 3.5% FLG'/TiO_2 could be obtained.

The effect of prolonged EG exfoliation and calcination process is also reflected in Raman and especially in XPS spectra.

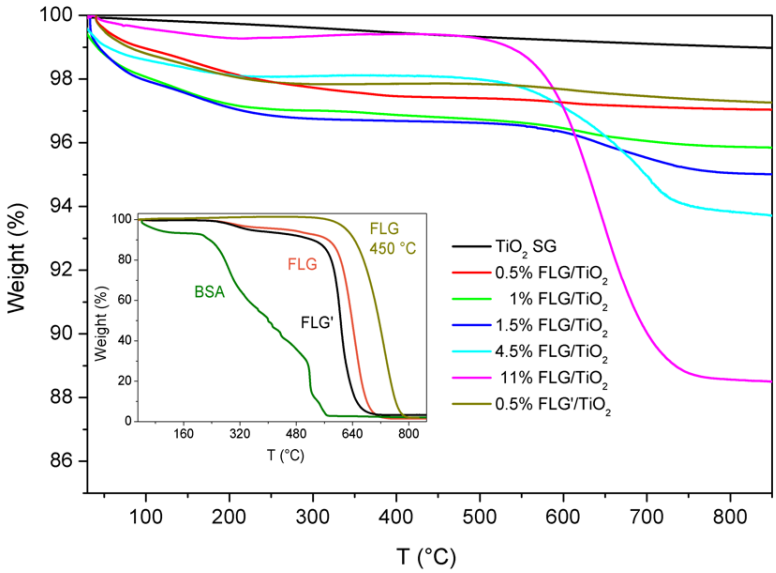

Figure 1. TGA curves of FLG/TiO_2 composites compared to bare TiO_2 SG. (Inset) TGA curves of FLG and BSA.

Figure 2 shows Raman spectra obtained for FLG, FLG' (fig. 2, top), TiO_2 SG and 0.5% FLG (FLG')/TiO_2 composites (fig. 2, bottom) that correspond to typical graphene-based and TiO_2 materials [43]. Additionally, the spectra of 1% FLG/TiO_2 and EG are included into SI (Fig. S2, SI). A relatively small amount of defects in FLG is reflected in Raman spectra by the ratio of peaks' intensities corresponding to defects and sp^2- graphitic C, *i.e.* I_D/I_G = 0.15 which consequently increases in FLG' to I_D/I_G = 0.22 [43, 44]. The relatively high ratio of I_{2D}/I_G suggests also relatively low number of sheets in FLG flakes. Likewise, low and variable number of sheets

is confirmed by the shape and position of 2D peak. According to the previously developed synthesis the present FLG should contain in average 5-7 sheets, while the presence of higher number, up to 10, as well as lower number, 2-4 sheets, can occur. In the presented spectra, fig. 2-top and fig. 2 top-inset, a 2D peak in FLG-b corresponds to the thicker flakes containing more than 5 sheets, while 2D peaks of FLG in FLG-a and FLG-c clearly indicate lower than 5 sheets number. In general, a 2D peak is formed by four sub-peaks. In thicker graphitic materials (and in graphite) the two sub-peaks at higher wavenumbers are much more pronounced that the two sub-peaks at lower wavenumbers, giving characteristic overall shape of 2D peak as it is the case for FLG-b in fig. 2 and for EG in fig. S2, SI[45]. On the contrary the 2D peak of monolayer graphene would appear as thin peak at lower wavenumbers. In FLG samples with the sheets number up to 5 (FLG-a and FLG-c), 2D peaks have consequently intermediary position and shape *i.e.* starting to shift toward lower wavenumbers being also more symmetrical compared to the peak of thicker flakes due to the increased intensity of low wavenumber sub-peaks. Concerning the composites, no significant shift of the peaks compared to the bare samples was identified.

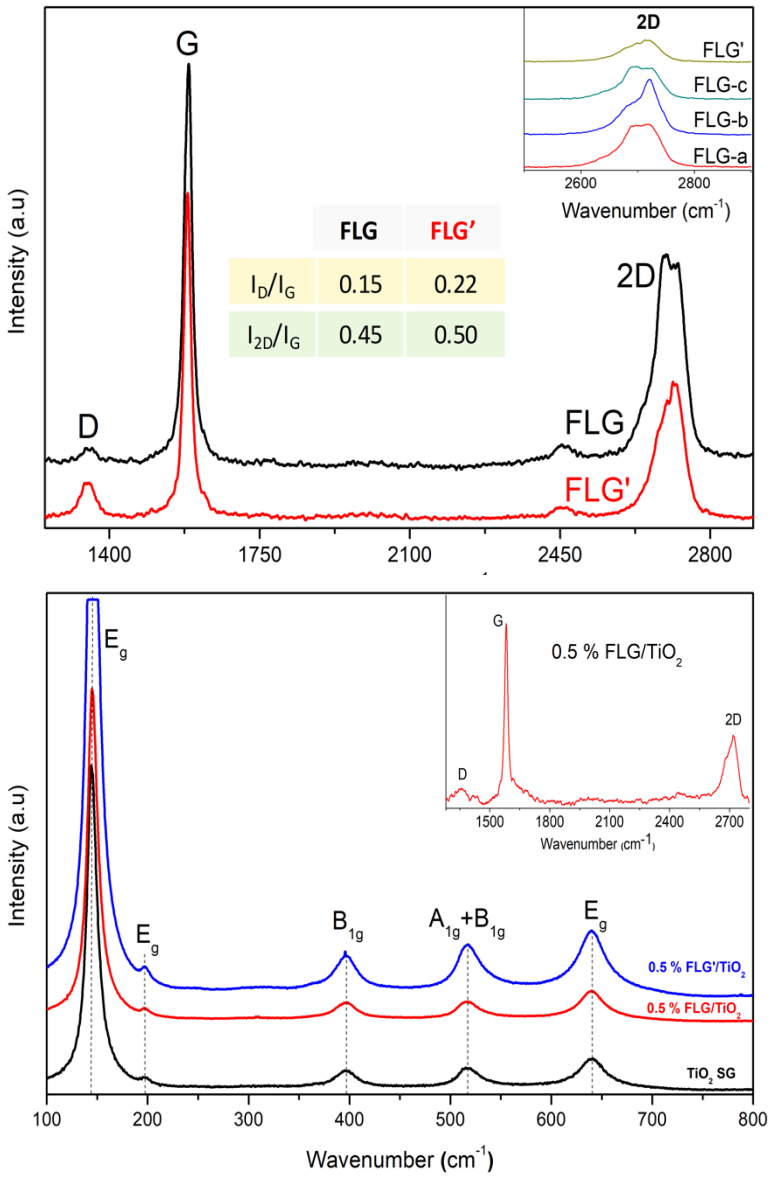

Figure 2. (Top) Raman spectra of FLG. (Inset): 2D bands of FLG on different flakes. (Bottom) Raman spectra of TiO_2 SG and 1% FLG/TiO_2 (Inset): Zoom of the 1200-2800 cm^{-1} region.

Concerning XPS spectra, C1s signal of bare FLG and FLG' (Fig. 3 a and Fig. S3, SI) exhibits the characteristic surface species related to oxygenated groups and defects in general, while their amount is relatively low compared to sp^2 C [46-48].

The C1s spectra changes drastically in the composites with low FLG loading with significant asymmetric enlargement of the peak (Fig. 3-b). This additional broadening of C1s peak reflects the enhancement of defects content in FLG (higher contribution of defects related sub-peaks) that is attributed to the effect of calcination performed at 450 °C. Likewise, the contribution of the peaks corresponding to oxygenated groups changes. As we can see below via TEM

microscopy, the edges of FLG are affected by the calcination process. It was shown earlier that the treatment in the presence of oxygen at this temperature provides high density of edges defects [48]. The effect of calcination depends on the FLG/TiO_2 ratio and since it is very significant at low FLG content, it decreases in the composites with higher FLG loading becoming negligible in 11% FLG/ TiO_2 and FLG alone (FLG 450°C). The C1s XPS spectra of the two latter samples as well as FWHM of all FLG containing composites are included in Fig. S4, SI. The FWHM is doubled almost in the composites with low FLG content and then quasi systematically decreases along with the increase of FLG in the samples. The FWHM of FLG and FLG-450°C are the same, 1.27, but certainly FLG-450°C does not contain BSA residue as confirmed by TGA analysis, while according to the TEM microscopy its edges are slightly affected by the calcination. We can clearly see also the appearance of new additional peak in the composite that can be assigned to –C-O-Ti- species (Fig. 3-b) [49,50], evidencing strong interaction between TiO_2 and FLG surface thanks to oxygenated –COO carbon species.

In Ti 2p XPS spectra of 1% FLG/TiO_2 composite (Fig. 3c), two typical Ti 2p peaks at 458.4 eV and 464.0 eV, respectively characteristic of Ti $2p_{3/2}$ and Ti $2p_{1/2}$ energies of Ti^{4+} in TiO_2, appear (Fig. 3c). The composite sample did not show any significant shift in these characteristic binding energies compared to bare TiO_2 SG (Fig. 3e), indicating that the presence of FLG did not induce significant chemical environment modification of Ti^{4+}. Concerning the O1s signal, the composite material (Fig. 3d) only shows the characteristic contribution of O^{2-} species of TiO_2 at 529.7 eV and of –OH surface groups at 531.6 eV, as observed also on bare TiO_2 SG (Fig. 3f), meaning that the addition of 1% of FLG did not modify the major surface oxygen species in detectable manner.

Looking at O/Ti atomic surface ratios (See Table S1, SI), it is observed that on TiO_2-containing sample, the stoichiometry between O and Ti is close to 2, as expected for TiO_2 materials with high TiO_2 loadings. Likewise, the C/Ti ratio increases when increasing the FLG content.

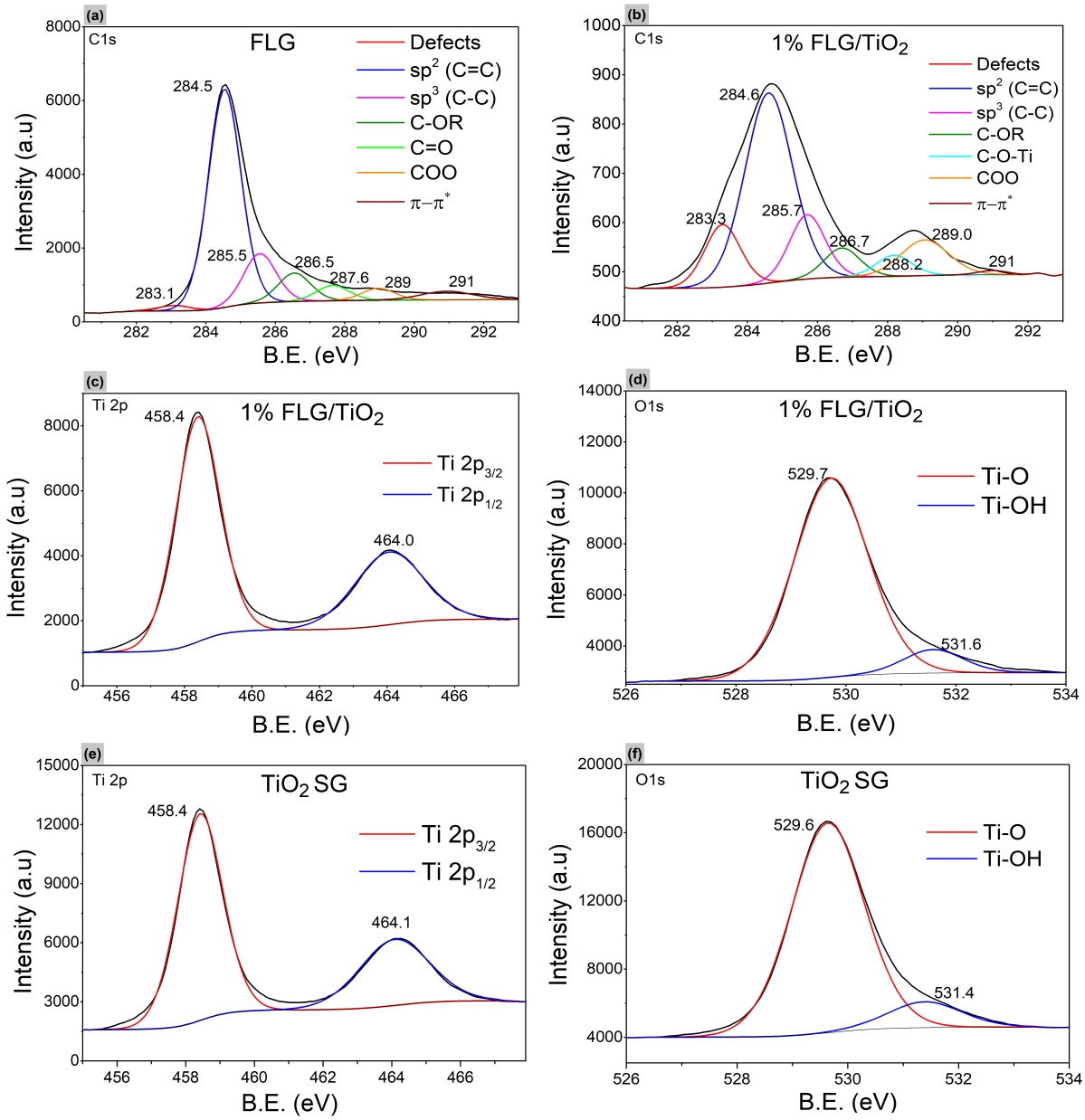

Figure 3. (a) XPS C1s spectra of bare FLG, (b)(c)(d) XPS C1s, Ti2p and O1s of 1% FLG/TiO_2 composite respectively, (e)(f) XPS Ti2p and O1s spectra of bare TiO_2 SG respectively.

From BET measurements, TiO_2 bare samples exhibited a type-IV adsorption-desorption isotherm profile characteristic of mesoporous solids with a uniform pore size distribution, whilst FLG (FLG')-based composites showed a type-II nitrogen adsorption-desorption profile related to macroporous solids. Compared to TiO_2 SG reference (103 m^2/g), specific surface area increases with FLG content to reach 136 m^2/g at 1 wt.% FLG, followed by a decrease at higher FLG contents to attain 88 m^2/g at 11 % FLG (Table 1 and Fig. 4, Fig. S5, SI). (The surface area of FLG' containing composite is slightly higher than the one for FLG composites (0.5 wt.%), table S2, SI). The specific surface enhancement is associated with an increase of pore width

and pore volume until reaching 1% FLG (Fig. 4-inset, Table 1). In the same manner, important diminution of surface area is the result of decrease of pore width and volume, pointing out the collapse of pore volume at 11% FLG, probably resulting from graphene layers stacking and leading to the small corresponding surface area, lower than for TiO_2 SG. The TiO_2 (P25 and UV 100) exhibited specific surface areas of 50 and 316 m^2/g, respectively.

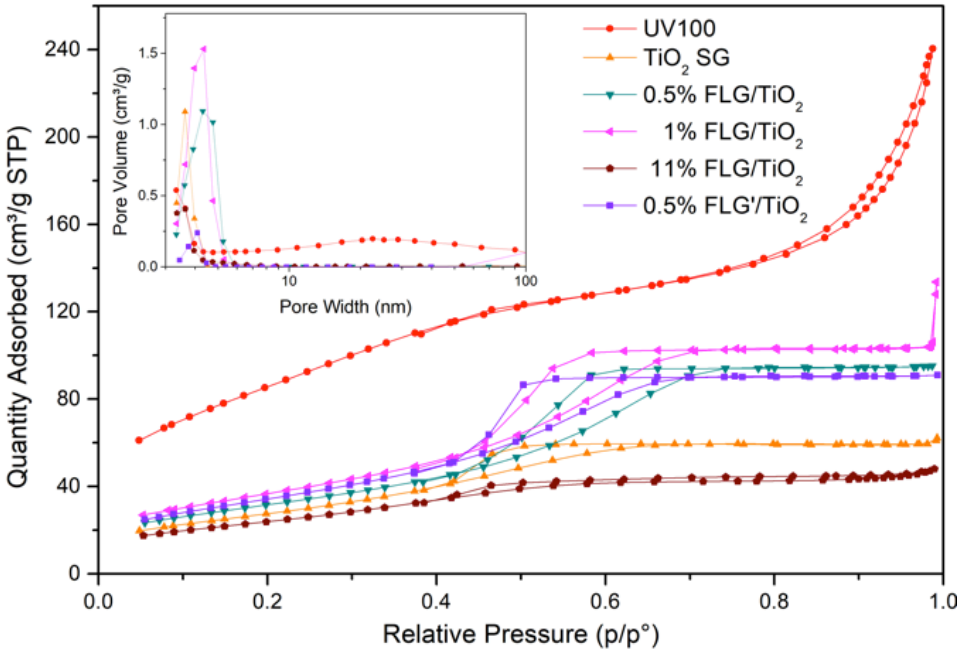

Figure 4. N_2 adsorption-desorption isotherms. (Inset) Pore volume distribution of selected FLG/TiO_2 composites and references.

TEM and SEM micrographs of 1% FLG/TiO_2 and 0.5% FLG'/ TiO_2 material are presented in Fig. 5. One can observe that well dispersed TiO_2 particles homogeneously cover the surface of FLG micrometric flakes and only locally the agglomeration of NPs appears (Fig. 5a, c). It is worthy to note that very high dispersion and homogenous planar distribution of NPs over FLG surface were still observed at much higher FLG loading, i.e. 11%, fig. S6., SI. At such high loading indeed FLG flakes are less affected by calcination treatment as it could be observed by TGA and XPS analysis. On the contrary, the local agglomeration of TiO_2 NPs in 0.5% and 1%FLG/TiO_2 can be related in some extend to the partially excessive burning of carbon and moving out of some NPs. The fig. 5b confirms the FLG layered structure constituted by *ca.* 7 layers of monoatomic graphene sheets with a lattice spacing of 0.34 nm in good accordance with that of the (002) plane of graphite [51]. Futhermore TiO_2 exhibits characteristic lattice spacing (0.35 nm) of (101) plane of TiO_2 anatase structure [52, 53]. TiO_2 nanoparticles sizes

are in the range of 10 nm, in agreement with the mean crystallite size determined from XRD measurements (Table 1). First of all, however, a good adhesion of TiO_2 NPs to FLG surface and edges is observed. The microscopy observations confirm as well the existence of enhanced defects density in FLG flakes in the form of jaggy edges that are an effect of calcination treatment, fig. 5d. Such edges, active side for the stabilization of TiO_2 species, are also present punctually at the FLG surface if belong to the upper sheets of the flakes. The locally observed excessive etching of the edges could be observed in 0.5 % FLG'/TiO_2 sample (fig. S7, SI). The additional representative SEM images of the composites, presented in fig. S8., SI illustrate the FLG flakes wrapped into TiO_2 agglomerates, while the flakes are covered by the layer of TiO_2 NPs.

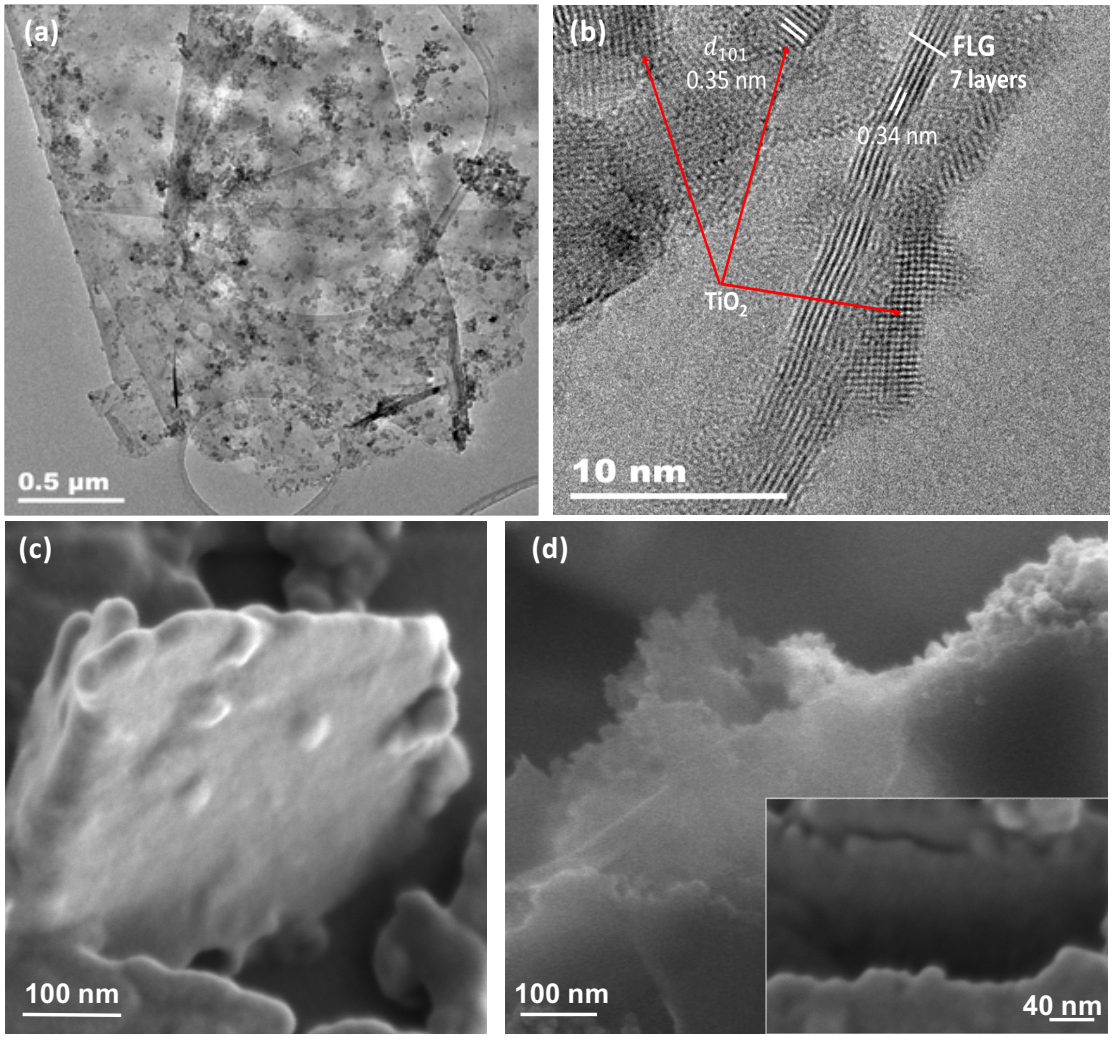

Figure 5. TEM and SEM micrographs of 1% FLG/TiO_2 and 0.5% FLG'/TiO_2 composite. Fig. 5a and c) demonstrates homogenous distribution of TiO_2 NPs over FLG flake. Fig. 5b) confirms good intimate interface between FLG and TiO_2. Fig. 5d) focuses on the jaggy FLG edges as an effect of calcination.

Samples	Plan (hkl)	2θ °	Cristallite size* (nm)	Surface Area** m²/g	Pore volume*** (cm^3/g)	Band gap energy (eV)
UV 100	(101)	25.7	9± 1	316 ± 6	0.25	3.3
P25		25.6	17± 1	54 ± 5	0.19	3.25
TiO_2 SG		25.5	11± 1	103 ± 5	0.08	3.0
0.5% FLG/TiO_2		25.4	11± 1	117 ± 5	0.16	3.0
1% FLG/TiO_2		25.5	11± 1	136 ± 6	0.22	3.0
1.5% FLG/TiO_2		25.4	11± 1	125 ± 5	0.19	3.0
4.5% FLG/TiO_2		25.5	10 ± 1	102 ± 5	0.06	2.9
11% FLG/TiO_2		25.5	12± 1	88 ± 4	0.04	2.7
0.5% FLG'/TiO_2		25.5	11± 1	128 ± 5	0.16	3.0

***Scherrer formula. ** Brunauer-Emmett-Teller (BET), *** Barrett-Joyner-Halenda (BJH)**

Table 1. Mean crystallite size, BET surface area, pore volume and band gap energy of FLG (FLG')/TiO_2 composites and references.

The XRD patterns of FLG/TiO_2 (and FLG'/TiO_2) composites are summarized in Fig. 6 and compared to TiO_2 SG, TiO_2 P25 and TiO_2 UV 100 references. The pattern of the as-prepared composites exhibits a major peak at *ca.* 25.4°, assigned to (101) planes in anatase phase in agreement with JCPDS file 21-1276. From mean crystallite size determination (*ca.* 11 nm, Table 1), no noticeable impact of neither FLG nor FLG' content is observed. Furthermore,

the presence of diffraction peak at *ca.* 26.6°, the main peak related to (002) planes of carbon graphitic phase, can be distinguished above 1.5 wt.% of FLG. For lower FLG content, the presence of FLG cannot be confirmed by means of DRX diffraction.

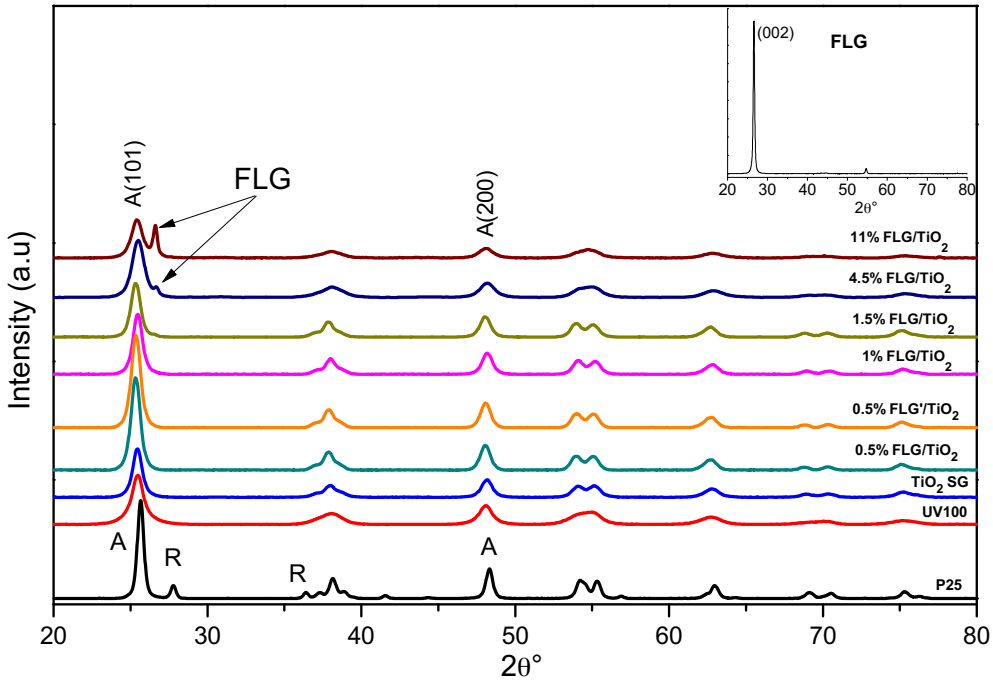

Figure 6. XRD pattern of FLG/TiO_2 compared to TiO_2 references and to (inset) bare FLG.

The UV-Vis absorption spectra (Fig. 7) show that on commercial TiO_2 UV 100 and P25, absorption occurs in the UV part of the spectra, corresponding to a band gap of 3.30 and 3.25 eV, respectively. It must be noticed that for P25, a tail of the absorption is observed until 415 nm, assigned to TiO_2 rutile contribution. One can also mention that the bare TiO_2 SG exhibits absorption in the blue region with a band gap of 3.0 eV. This phenomenon may be related to defective TiO_2 structure as calcination was performed at a moderate temperature of 450 °C in order to prevent excessive FLG degradation in the composite samples. This assumption is confirmed by UPS analyses evidencing the presence of densities of states close to the Fermi level. Looking at the composite materials, one can clearly distinguish TiO_2 and FLG contributions. In addition to TiO_2 absorption, a broad background absorption proportionally increasing with FLG content is observed in the visible range and can thus be attributed to the presence of carbon [54]. It seems also that the introduction of defect/oxygen functionalities during the calcination into the FLG affects the UV-Vis spectroscopy of FLG, the FLG-450°C having clearly much higher absorption intensity, fig. S9, SI.

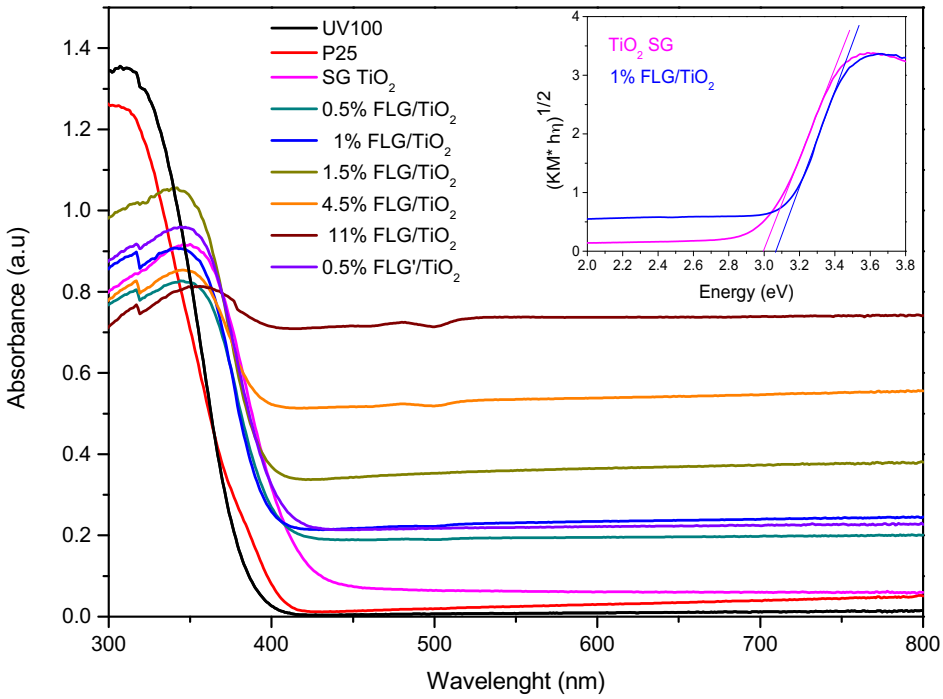

Figure 7. Diffuse reflectance absorption of FLG/TiO_2 composites and references. (Inset) Tauc plot for the determination of the band gap of selected samples.

From UPS spectra (Fig. S10), one can observe that bare TiO_2 SG has densities of states close to the Fermi level, which might be attributed to the presence of oxygen vacancies/defects in TiO_2 crystalline structure, as a result of moderate TiO_2 calcination temperature. It must also be mentioned that the densities of states for TiO_2 SG, 1% FLG/TiO_2 and 0.5% FLG'/ TiO_2 are located at lower binding energies than for 0.5% FLG/TiO_2 sample. From combining UV-Vis (band-gap determination) and UPS (VBmax measurements) analyses, a schematic band structure could be deduced (Fig. 8). From this schematic band structure, it can be assumed that from an energetically point of view the main studied samples fulfill the requirements for H_2O oxidation and methanol reforming (that is less evident for 0.5% FLG'/TiO_2). Likewise, only the photogenerated electrons on the conduction band of the 0.5% FLG/TiO_2 composite may be able to reduce H^+ into H_2.

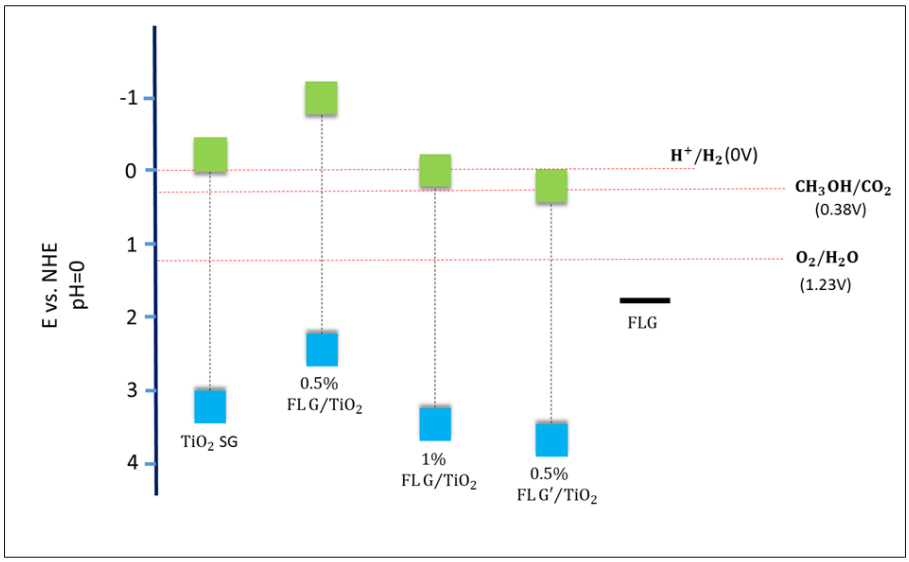

Figure 8. Schematic band gap energies and band positions of TiO_2 SG, 0.5% FLG/TiO_2, 1% FLG/TiO_2, 0.5% FLG'/TiO_2 composites and FLG deduced from UV-Vis and UPS measurements.

Photocatalytic performance

The time course of H_2 production was measured *in situ*. After switching on the lamp, H_2 production gradually increased to reach a plateau which was stable during at least the duration of the photocatalytic tests, *i.e.* for 3 h. In Fig. 9-top, H_2 production rates were thus considered as the average value on this stable plateau. It can be seen from the figure that in most cases the concentration of the suspended photocatalyst has an impact on the photocatalytic H_2 production rate, the lower concentration (0.1 g/L) leading to the highest activity. Indeed, the decrease in H_2 production activity when doubling the photocatalyst concentration in suspension may also be due to light screening phenomena and/or scattering occurring at intra and interparticle [55]. Considering activity of TiO_2 samples, TiO_2 P25 exhibits the best reaction rate, twice more important than the one observed on the TiO_2 SG photocatalyst. The addition of FLG to TiO_2 SG results in an increase of activity in all composites compared to TiO_2 SG. 1% FLG/TiO_2 composite yields the highest performance amongst all the FLG-based composites, with almost twice enhanced H_2 production rate (265 µmol/h.g) compared to the best TiO_2 P25 reference (150 µmol/h.g). Looking at the global quantum yield (at 0.1 g/l of photocatalyst concentration, Fig. 9-bottom), the corresponding values follow the same tendency reaching 0.016% value for the 1% FLG/TiO_2, which is almost 2 and 3 times higher than the yield

observed for TiO_2 P25 and UV 100 respectively. Comparing with the bare TiO_2 SG, one can see the beneficial impact of association with FLG material in all composites. Likewise, an effect of the calcination on FLG can be observed in FLG-450°C by increasing H_2 production from 16 to 71 μmol/h.g., (Fig. S11., SI). The activities of the photocatalysts do not change however in a linear manner as a function of FLG content. Since FLG/TiO_2 with 1 wt.% FLG is more active than the composite with 0.5% of FLG, the activity with the additional 0.5% *i.e.* 1.5% FLG decreases being enhanced again at loading of 4.5%, and next decreased at loading of 11%. This lack of correlation (for each FLG loading the test was running twice with freshly prepared materials) can be explained by the fact that several factors affect the composites' activity. Higher FLG loading would result in higher visible light absorption and better charge separation, but higher light scattering and screening will appear (each additional sheet in FLG makes reduction of transparency by 2.3%). Likewise, not only the amount of FLG but related dispersion degree of FLG plays an important role. Since the present FLG is relatively low defect-type of graphene material (large microscopic sheets with well crystalized lattice), lower amount of FLG in the composites ensures higher dispersion of FLG and consequently higher dispersion of TiO_2 as well. This is in accordance with the specific surface area and porosity measurements (table 1). The FLG amount has to be however sufficient to attached TiO_2 precursor/NPs at most active, defective sites to form intimate interface contact with NPs. In accordance with the best performance, 1% FLG/TiO_2 has the highest surface area within all composites. Concerning the composites containing FLG', the same tendency of hydrogen production rate, as it is in FLG composites, is observed (fig. S12., SI). All composites are more active than the reference TiO_2 SG and activity do not increase in linear manner with FLG' content but two most active samples arise with the best one at FLG' loading of only 0.5%. (Consequently, the second most active composite in the FLG' composites family contains 2.5% of FLG', SI). This shows that increased amount of edges defects in FLG' allows to obtain the same activity at lower graphene content. It permits to stabilize and form efficient interface with higher amount of TiO_2 species. Likewise, still other very important factor relates to defects and oxygen reach groups such as hydroxyl, carbonyl or carboxyl that are introduced additionally into the FLG flakes by the calcination treatment of the composites. As mentioned above their introduction strongly depends on the ratio of TiO_2 to FLG, where, according to the XPS spectroscopy, it is significant and very small at low and the highest FLG % respectively. Such "defected" carbon not only helps to disperse and form the stable interface with TiO_2 NPs but enhances also the adsorption of MeOH. The significant adsorption of MeOH between two neighbors hydroxyl groups and next considerable adsorption of MeOH on less active groups on

functionalized graphite were recently claimed.[56] Beside the role of NPs attachment and chemisorption sites, the defects/functional groups on graphene are desired for increasing a tunneling probability i.e. to enhanced the visible light activity but their amount should be reasonable to ensure on the other hand a transport channels inhibiting electron-hole recombination rate.[57] The additional curve of time-on-stream of hydrogen production for 1% FLG/TiO_2 photocatalyst as well as stability investigations of this sample, i.e. DRX analysis of spent catalysts and recycling test are presented in SI (Fig. S13.-S15.).

It is worthy to highlight that comparing to literature, the performance of 1 and 0.5% FLG (and FLG' respectively)/TiO_2 in methanol photoreforming is very high considering such low FLG %. For instance, an addition of rGO to TiO_2 in the best sample (optimized % of rGO and GO reduction manner) showed one order of magnitude enhancement of activity but at 20% of rGO [58]. Concerning low rGO % content, 1% rGO-TiO_2 composite indeed showed excellent activity to produce H_2 from water but TiO_2 is present in this catalysts in the form of sheets; the interface with rGO and active surface of TiO_2 is then incomparably higher than the one with NPs [59].

Taking into account here that the band gap of the investigated composites and absorption in the visible range is modified mostly only at higher FLG content (table 1), the impact of FLG on activity related to improvement of absorption properties in the best samples are not obvious. Clearly however, the present FLG may result in great advantage of charge transport properties due to large and well-crystalized carbon lattice together with its incomparably simple synthesis. In order to check charge carriers' generation and transport in the composites, TRMC analysis were performed (below, part 3.3).

Concerning the photoreforming reaction, it is generally assumed that photoreforming of alcohols on TiO_2-based materials can occur by the stepwise oxidation of water by photoinduced holes, to produce radicals which can abstract an alpha-hydrogen leading to the formation of °RCH_2-OH radical that is further oxidized to an aldehyde, carboxylic acid, and CO_2 [60, 61]. The hydrogen atoms from the alpha carbon could be easily extracted and evolved in the form of H_2.

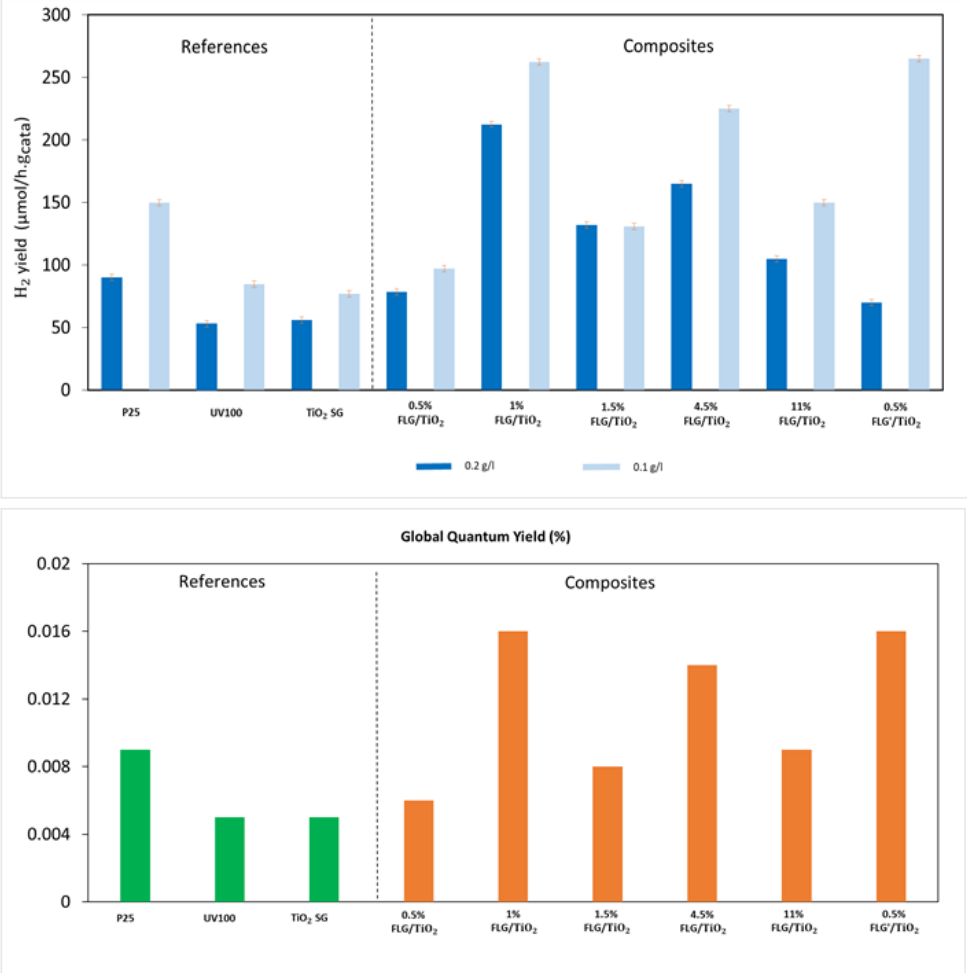

Figure 9. (top) Mass hydrogen production rate (concentration of the photocatalyst in the reaction media: 0.2 g/L and 0.1 g/L), and (bottom) global quantum yield (0.1 g/L).

However, it is also admitted that the oxidation steps can proceed via another path involving OH° attack [62]. In the presence of a co-catalyst, it is widely assumed that the successive oxidation steps take place by the photogenerated holes in the VB of the semiconductor, while H_2 evolution proceeds on the co-catalyst [63]. Some authors also suggested a participation of the co-catalyst in the dehydrogenation/decarbonylation of the sacrificial agent [64] or acting as recombination centre of H-atoms [65]. Consequently, without the presence of a metal co-catalyst in our case, we can suspect the following stepwise oxidation of methanol on the surface of TiO_2 by photogenerated holes, releasing protons and forming HCOH and eventually HCOOH (the presence of these intermediates was not however checked).[63, 66].

$$H_2O + h^+ \rightarrow OH° + H^+$$
$$CH_3OH + OH° \rightarrow CH_2OH° + H_2O$$

$CH_2OH^\circ \rightarrow HCHO + H^+ + e^-$
$2\,H^+ + 2\,e^- \rightarrow H_2$
$HCHO + H_2O \rightarrow HCOOH + H_2$
$HCOOH \rightarrow CO_2 + H_2$

Overall reaction : $CH_3OH + H_2O \rightarrow CO_2 + 3\,H_2$

Electron mobility measurements by Time Resolved Microwave Conductivity (TRMC)

Fig. 10a shows normalized TRMC measurements of the most active 1% FLG/TiO_2 sample, the lowest FLG-containing composite 0.5% FLG (FLG')/TiO_2, bare TiO_2 SG and FLG, at 360 and 450 nm laser excitation. In bare samples, we can clearly distinguish two typical regions of electrons recombination, the first one with rapid decay and the second region with a much slower decay. As commonly accepted we estimate that the second region starts certainly at the most at 40 ns after maximum value of I. According to their structural features, bare FLG leads to the most efficient charge carriers' generation at 450 nm, while TiO_2 SG at 360 nm. From these results it must be mentioned that only FLG and FLG' allows the generation of charge carriers under visible light activation. Contrary to FLG, the generation of charge carriers in FLG' at 360 nm is considerable but extremely unstable, what can be related to high number of trapping defects. For the same reason high instability of the signal is measured for FLG' at 450 nm. Likewise, the fast first region decay is clear in bare samples (I_{40ns}/I_{max} = 0.7 at 450 nm for FLG, I_{40ns}/I_{max} = 0.55 and 0.78 at 360 for TiO_2 SG and P25 respectively (curve not shown here). Since generation of charge carriers is not clearly measurable in 0.5% FLG/TiO_2, 1% FLG/TiO_2 and 0.5% FLG'/TiO_2 composites create detectable charge carriers with enough lifetime of the photogenerated carriers after excitation at 360 nm (fig. 10b). Moreover, one sample, 1% FLG/TiO_2, reveals a slight increase of the signal in the second region (I_{40ns}/I_{max} = 0.5 and $I_{0.9\mu s}/I_{40ns}$= 1). Relatively stable signal compared to the bare samples is detected also in 0.5%FLG'/TiO_2 (I_{40ns}/I_{max} = 0.67 and $I_{0.9\mu s}/I_{40ns}$= 0.72). More generally one can mention that the FLG composites show less intense TRMC signal meaning that less charge carriers are produced compared to bare TiO_2 (at 360 nm) or to FLG (at 450 nm). These phenomena can be explained respectively by means of photons (UV) absorption by TiO_2 followed by electrons injection and trapping, and by (visible light) photons absorption by FLG, followed by electrons injection and thus trapping. In both cases, it may be supposed that electron trapping occurs at TiO_2/FLG interface. The behaviour of FLG' composite at 360 nm on the other hand, with

relatively high and stable signal, indicates good interface between FLG' and TiO_2. The abundant defects causing the extensive trapping of the photogenerated charges in FLG' in the composites are occupied forming interface with TiO_2. Moreover, it is important to highlight that the TRMC signal corresponding to the 1% FLG/TiO_2 composite material exhibits a pronounced contribution at *ca.* 0.5 μs corresponding to the appearance of increased mobile electrons density that may be attributed to electron injection either from TiO_2 to FLG (at 360 nm) or from FLG to TiO_2 (at 450 nm). As the photocatalytic activity of 1% FLG/TiO_2 sample exhibited enhanced H_2 production properties one may suppose that, even if there is a loss of electron mobility compared to bare materials, the free photogenerated electrons are trapped more rapidly at TiO_2/FLG interface due to the presence of conductive FLG sheets interfaced in an optimized way with nanoparticles at 1% FLG loading, thus leading to better charges separation and enhancement of lifetime of charge carriers. Consequently, enhanced H_2 production rate takes place using more efficiently holes for methanol oxidation and trapped electrons for H^+ reduction into H_2. Additionally, when activating with solar light (UV + visible) one may underline an additional charges photogeneration from FLG material.

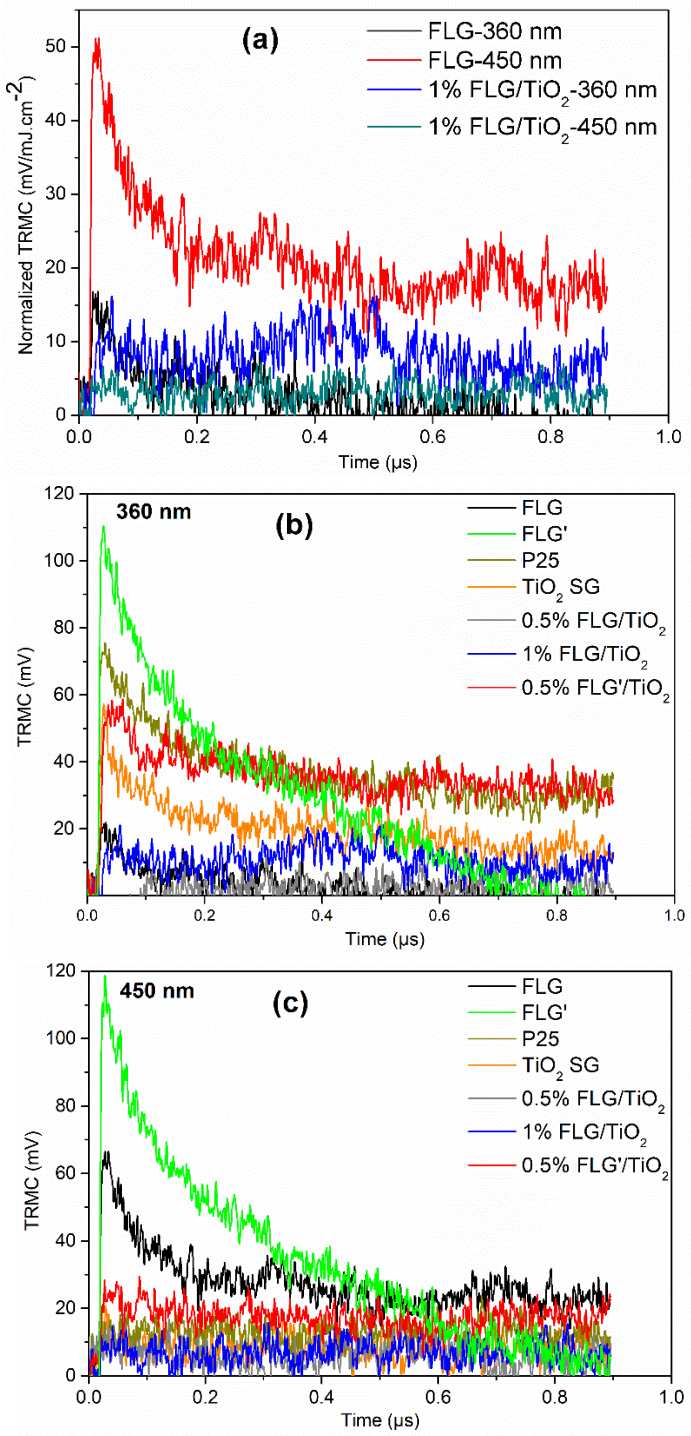

Figure 10. Time course of TRMC signals of FLG, TiO_2 SG, 0.5%/1% FLG/TiO_2 and 0.5% FLG'/TiO_2 composites: **(a)** normalized to the energy density at different wavelengths **(b)** under 360nm pulse laser excitation and **(c)** under 450nm pulse laser excitation.

Conclusion

The series of FLG/TiO_2 composites with different FLG loadings (0.5-11 wt.%), and additionally with lower FLG flakes size (FLG'), were investigated as photocatalysts without addition of co-catalyst towards hydrogen production from methanol under solar light irradiation. All composites showed higher activity than FLG and bare TiO_2 SG samples. The highest performance with activity three times and twice higher than the reference and commercial TiO_2 respectively was achieved for the composites with low FLG loading, i.e. 1% FLG/TiO_2 and 0.5% FLG'/TiO_2. The resulting enhanced hydrogen production was investigated via analysis of morphology, chemistry, optical and electronic structures of the composites. We relate the highest activity of 1% FLG/TiO_2 and 0.5% FLG'/TiO_2 to the reduction of charge carriers' recombination thanks to the electron trapping effect of well interfaced TiO_2 NPs/FLG sheets as well as to enhanced accessible surface area and additional FLG visible light absorption properties. It was also shown that the calcination of the composites as well as prolonged exfoliation of initial graphite, both providing enhancement of defects/functionalization in FLG, lead to stabilization and formation of the efficient interface between TiO_2 and FLG. Likewise, FLG with enhanced edges defects content (FLG') is more quantitatively performant than FLG. The optimized interface was confirmed by XPS and TEM analysis, while its impact on enhancement of charge carriers' lifetime was observed in TRMC analysis.

Author contributions Hamza El Marouazi: data curation, formal analysis, methodology, conceptualization, investigation, visualization, validation, P. Jiménez-Calvo: formal analysis, investigation, E. Breniaux: data curation, formal analysis, investigation, C. Colbeau-Justin: data curation, formal analysis, investigation, validation (TRMC), I. Janowska: conceptualization, methodology, investigation, supervision, validation, writing, resources, visualization, V. Keller: conceptualization, methodology, investigation, supervision, validation, writing, resources, project administration.

Funding: The work was performed in the frame of PHOTER project, l'Agence Nationale de la Recherche (ANR) is acknowledged for the financial support (N° ANR-17-CE06-0011-02).

Acknowledgements

Walid Baazis is acknowledged for carrying out TEM images at IPCMS (UMR 7504 CNRS-UDS), Strasbourg. Frédéric Antoni is acknowledged for sharing Raman spectrometer at Icube

(UMR 7357, CNRS-UDS), Strasbourg. We thank also Vasiliki Paphaminou (ICPEES) for performing XPS and UPS measurements.

Present address

Edouard Breniaux : CIRIMAT-UPS-CHIMIE Université Toulouse 3 - Paul Sabatier , 118 Route de Narbonne , 31062 Toulouse cedex 09 ,France

Pablo Jiménez-Calvo : Laboratoire de Physique des Solides-UMR 8502 CNRS-Université Paris-Saclay, 1 rue Nicolas Appert, 91405 Orsay Cedex-France

Appendix A. Supplementary data

Supplementary material related to this article can be found, in the online version, at doi:

References

1. Tong, H.; Ouyang, S.; Bi, Y.; Umezawa, N.; Oshikiri, M.; Ye, J., Nano-photocatalytic materials: possibilities and challenges. Adv. Mater. **2012**, 24, 229-251. doi.org/10.1002/adma.201102752.

2. Chen, X.; Mao, S.S., Titanium dioxide nanomaterials: synthesis, properties, modifications, and applications. Chem. Rev. **2007**, 107, 2891-2959. doi.org/10.1021/cr0500535.

3. Fujishima, A.; Honda, K., Electrochemical photolysis of water at a semiconductor electrode. Nature **1972**, 238, 37-38. doi.org/10.1038/238037a0.

4. Linsebigler, A.L.; Lu, G.; Yates, J.T., Photocatalysis on TiO_2 surfaces: principles, mechanisms, and selected results. Chem. Rev. **1995**, 95 ,735-758. doi.org/10.1021/cr00035a013.

5. Luciani, G; Imparato, C; Vitiello. Photosensitive Hybrid Nanostructured Materials: The Big Challenges for Sunlight Capture, Catalysts **2020**, 10, 103. doi.org/10.3390/catal10010103.

6. Zhang, J; Zhu, Q; Wang , L; Nasir, M; Cho, S.-H; Zhang J. g-C3N4/CoAl-LDH 2D/2D hybrid heterojunction for boosting photocatalytic hydrogen evolution. Int. J. Hydr. En. **2020**, 45 (41), 21331-21340. doi.org/10.1016/j.ijhydene.2020.05.171.

7. Jimenez-Calvo, P.; Marchal, C.; Cottineau, T.; Caps, V.; Keller, V., Influence of the gas

atmosphere during the synthesis of g-C3N4 for enhanced photocatalytic H_2 production from water on Au/g-C3N4 composites. J. Mater. Chem. A **2019**, 7, 14849-14863. doi.org/10.1039/C9TA01734H.

8. Zhang, N.; Zhang, Y.; Xu, Y.-J., Recent progress on graphene-based photocatalysts: current status and future perspectives. Nanoscale **2012**, 4, 5792-5813. doi.org/10.1039/C2NR31480K.

9. Tan, L.-L.; Chai, S.-P.; Mohamed, A.R., Synthesis and applications of graphene‐based TiO_2 photocatalysts. ChemSusChem **2012**, 5, 1868-1882. doi.org/10.1002/cssc.201200480.

10. Leary, R.; Westwood, A., Carbonaceous nanomaterials for the enhancement of TiO_2 photocatalysis. Carbon **2011**, 49, 741-772. doi.org/10.1016/j.carbon.2010.10.010.

11. Zhang, X.-Y.; Li, H.-P.; Cui, X.-L.; Lin, Y., Graphene/ TiO_2 nanocomposites: synthesis, characterization and application in hydrogen evolution from water photocatalytic splitting. J. Mat. Chem. **2010**, 20, 2801-2806. doi.org/10.1039/B917240H.

12. Kim, H.; Moon, G.; Monllor-Satoca, D.; Park, Y.; Choi, W., Solar photoconversion using graphene/ TiO_2 composites: nanographene shell on TiO_2 core versus TiO_2 nanoparticles on graphene sheet. J. Phys. Chem. C. **2012**, 116, 1535-1543. doi.org/10.1021/jp209035e.

13. Giovanetti, R.; Rommozzi, E.; Zannotti, M.; D'Amato, C.A., Recent advances in graphene based TiO_2 nanocomposites (G TiO_2Ns) for photocatalytic degradation of synthetic dyes. Catalysts **2017**, 7, 305-339. doi.org/10.3390/catal7100305.

14. Zhang, X.-Y.; Li, H.-P.; Cui, X.-L.; Lin, Y., Graphene/ TiO_2 nanocomposites: synthesis, characterization and application in hydrogen evolution from water photocatalytic splitting. J. Mater. Chem. **2010**, 20, 2801-2806. doi.org/10.1039/B917240H.

15. Xiang, Q.; Yu, J., Enhanced photocatalytic H_2-production activity of graphene-modified titanianosheets. Nanoscale **2011**, 3, 3670-3678. doi.org/10.1039/C1NR10610D.

16. Liu, J.; Bai, H.; Wang, Y.; Liu, Z.; Zhang, X.; Sun, D.D., Self-assembling TiO_2 nanorods on large graphene oxide sheets at a two-phase interface and their anti-recombination in photocatalytic applications. Adv. Funct. Mater. **2010**, 20, 4175-4181. doi.org/10.1002/adfm.201001391.

17. Nair, R.R.; Blake, P.; Grigorenko, A.N.; Novoselov, K.S.; Booth, T.J.; Stauber, T.; Peres, N.M.R.; Geim, A.K., Fine structure constant defines visual transparency of graphene. Science **2008**, 320, 1308. doi.org/10.1126/science.1156965.

18. Xiang, Q.; Yu, J.; Jaroniec, M., Graphene-based semiconductor photocatalysts. Chem. Soc. Rev. **2012**, 41, 782-796. doi.org/10.1039/C1CS15172J.

19. Novoselov, K.S.; Geim, A.K.; Morosov, S.V.; Jiang, D.; Zhang, Y.; Dubonos, S.V.; Grigorieva, L.V.; Firsov, A.A., Electric field effect in atomically thin carbon films. Science **2004**, 306, 666-669. doi.org/10.1126/science.1102896.

20. Berger, C.; Song, Z.; Li, X.; Wu, X.; Brown, N.; Naud, C.; Mayou, D.; Li, T.; Haas, J.; Marchenkov, A.N.; Conrad, E.H.; First, P.N.; De Heer, P.N., Electronic confinement and coherence in patterned epitaxial graphene. Science **2006**, 312, 1191-1196. doi.org/10.1126/science.1125925.

21. Peplow, M., Graphene: the quest for supercarbon. Nature **2013**, 503, 327-329. doi.org/10.1038/503327a.

22. Sordello, F.; Zeb, G.; Hu, K.; Calza, P.; Minero, C.; Szkopeke, T.; Cerruti, M., Tuning TiO_2 nanoparticle morphology in graphene–TiO_2 hybrids by graphene surface modification. Nanoscale **2014**, 6, 6710-6719. doi.org/10.1039/C4NR01322K.

23. Anfosi, L.; Calza, P.; Sordello, F.; Giovannoli, C.; Di Nardo, F.; Passini, C.; Cerruti, M.; Goryacheva, I.Y.; Speranskaya, E.S.; Baggiani, C., Multi-analyte homogenous immunoassay based on quenching of quantum dots by functionalized graphene. Anal. Bioanal. Chem **2014**, 406, 4841-4849. doi.org/10.1007/s00216-014-7885-6.

24. Liang, Y.; Wang, H.; Sanchez Casalongue, H.; Chen, Z.; Dai, H., TiO_2 nanocrystals grown on graphene as advanced photocatalytic hybrid materials. Nano Res. **2010**, 3, 701-705. doi.org/10.1007/s12274-010-0033-5.

25. Song, J.; Ling, Y.; Xie, Y.; Liu, L.; Zhu, H., One-pot engineering TiO_2/graphene interface for enhanced adsorption and photocatalytic degradation of multiple organics. Nanotechnology **2018**, 29, 395701. doi.org/10.1088/1361-6528/aacc56.

26. Schniepp, H.C.; Li, J.L.; McAllister, M.J.; Sai, H.; Herrera-Alonso, M.; Adamson, D.H.; Prud'homme, R.K.; Car, R.; Saville, D.A.; Aksay, I.A., Functionalized single graphene sheets derived from splitting graphite oxide. J. Phys. Chem. B **2006**, 110, 8535-8539. doi.org/10.1021/jp060936f.

27. Xao, X.; Jang, J.; Nagase, S., Hydrazine and thermal reduction of graphene oxide: reaction mechanisms, product structures, and reaction design. J. Phys. Chem. C. **2010**, 114, 832-842. doi.org/10.1021/jp909284g.

28. Ramesha, G.K.; Sampath, S., Electrochemical reduction of oriented graphene oxide films: an in situ Raman spectroelectrochemical study. J. Phys. Chem. C. **2009**, 113, 7985-7989. doi.org/10.1021/jp811377n.

29. Voiry, D.; Yang, D.; Kupferberg, J.; Fullon, R.; Lee, C.; Jeong, H.Y.; Shin, H.S.; Chhowalla, M., High-quality graphene via microwave reduction of solution-exfoliated graphene oxide. Science **2016**, 353, 1413-1416. doi.org/10.1126/science.aah3398.

30. Golsheikh, A.M.; Lim, H.N.; Zakaria, R.; Huang, N.M., Sonochemical synthesis of reduced graphene oxide uniformly decorated with hierarchical ZnS nanospheres and its enhanced photocatalytic activities. RCS Adv. **2015**, 5, 12726-12735. doi.org/10.1039/C4RA14775H.

31. Ng, Y.G.; Lightcap, Y.G; Goodwin, K.; Matsumura, M.; Kamat, P.V., To what extent do graphene scaffolds improve the photovoltaic and photocatalytic response of TiO_2 nanostructured films. J. Phys. Chem. Lett. **2010**, 1, 2222-2227. doi.org/10.1021/jz100728z.

32. Zhang, H.; Lv, X.; Li, Y.; Wang, Y.; Li, J., P25-graphene composite as a high performance photocatalyst. ACS Nano **2009**, 4, 380-386. doi.org/10.1021/nn901221k.

33. Chua, C.K.; Pumera, M., Chemical reduction of graphene oxide: a synthetic chemistry viewpoint. Chem. Soc. Rev. **2014**, 43, 291-312. doi.org/10.1039/C3CS60303B.

34. Park, S.; Ruoff, R.S., Chemical methods for the production of graphenes. Nature Nanotech. **2009**, 4, 217-224. doi.org/10.1038/nnano.2009.58.

35. Szabo, T.; Berkesi, O.; Forgo, P.; Jesepovits, K.; Sanakis, Y.; Petridis, D.; Dekany, I., Evolution of surface functional groups in a series of progressively oxidized graphite oxides. Chem. Mater. **2006**, 18, 2740-2749. doi.org/10.1021/cm060258+.

36. Minella, M.; Demontis, M.; Sarro, M.; Sordello, F.; Calza, P.; Minero, C.; Photochemical stability and reactivity of graphene oxide. J. Mater. Sci. **2015**, 50, 2399-2409. doi.org/10.1007/s10853-014-8791-1.

37. Zahibi, C.; Ahmadian-yazdi, M.R.; Eslamian, M.R., Photocatalytic graphene- TiO_2 thin films fabricated by low-temperature ultrasonic vibration-assisted spin and spray coating in a sol-gel process. Catalysts **2017**, 7, 136. doi.org/10.3390/catal7050136.

38. Ba, H.; Truong-Phuoc, L.; Pham-Huu, C.; Luo, W.; Baaziz, W.; Romero, T.; Janowska, I., Colloid approach to the sustainable top-down synthesis of layered materials. ACS Omega **2017**, 2, 8810-8617. doi.org/10.1021/acsomega.7b01311.

39. Kouamé, N. A.; Robert, D.; Keller, V.; Keller, N.; Pham, C.; Nguyen, P., Preliminary study of the use of β-SiC foam as a photocatalytic support for water treatment. Catal. Today **2011**, 161, 3-7. doi.org/10.1016/j.cattod.2010.10.045.

40. Scofield, J.H., Hartree-Slater subshell photoionization cross-sections at 1254 and 1487 eV. J. Electron Spectros. Relat. Phenomena **1976**, 8, 129-137. doi.org/10.1016/0368-2048(76)80015-1.

41. Tahiri Alaoui, O. ; Herissan, C. ; Le Quoc, M.E. ; Zekri, M.E.M; Sorgues, S.; Remita, H.; Colbeau-Justin, C., Elaboration, charge-carrier lifetimes and activity of Pd-TiO_2 photocatalysts obtained by gamma radiolysis. J. Photochem. Photobiol. A. **2012**, 242, 34-43. doi.org/10.1016/j.jphotochem.2012.05.030.

42. Colbeau-Justin, C.; Kunst, M.; Huguenin, D., Structural influence on charge-carrier lifetimes in TiO_2 powders studied by microwave absorption. J. Mater. Sci. **2003**, 38, 2429-2437. doi.org/10.1023/A:1023905102094.

43. Bykkam, S.; Rao, K.V.; Naresh Kumar, R.; Chakra, Ch.S.; Dayakar, T., Few-layered graphene decked with TiO_2 nano particles by ultrasonic assisted synthesis and its dye-sensitized solar cell application. J Mater Sci: Mater Electron **2016**, 27, 12574-12581. doi.org/10.1007/s10854-016-5388-2.

44. Ni, Z.; Wang, Y.; Yu, T.; Shen, Z., Raman spectroscopy and imaging of graphene. Nano Res. **2008**, 1, 273-293. doi.org/10.1007/s12274-008-8036-1.

45. Ferrari, A. C.; Meyer, J. C.; Scardaci, V.; Casiraghi, C.; Lazzeri, M.; Mauri, F.; Piscanec, S.; Jiang, D.; Novoselov, K. S.; Roth, S.; Geim, A. K., Raman spectrum of graphene and graphene layers. Phys. Rev. Lett. **2006**, 97, 187401. doi.org/10.1103/PhysRevLett.97.187401.

46. Blyth, R.I.R. ; Buqa , H. ; Netzer F.P. ; Ramsey, M.G. ; Besenhard, J.O. ; Golob, P. ; Winter, M., XPS studies of graphite electrode materials for lithium ion batteries. Appl. Surf. Sci. **2000**, 167, 99-106. doi.org/10.1016/S0169-4332(00)00525-0.

47. Pirzado, A.A. ; Truong-Phuoc L. ; Papaefthimiou, V. ; Matei Ghimbeu, C. ; Le Normand, F. ; Ba, H.; Thanh-Tung, T. ; Pham-Huu, C. ; Janowska I., Activation of few layer graphene by μW-assisted oxidation in water via formation of nanoballs – Support for platinum nanoparticles. J. Colloid Interface Sci. **2015**, 451, 221–230. doi.org/10.1016/j.jcis.2015.03.063.

48. Janowska, I.; Lafjah, M.; Papaefthymiou, V.; Pronkin, S.; Ulhaq-Bouillet, C., Edges fractal approach in graphene-Defects density gain. Carbon **2017**, 123, 395-401. doi.org/10.1016/j.carbon.2017.07.077.

49. Panchangam, S.C.; Yellatur, C.S.; Yang, J.-S. ; Loka, S.S.; Lin, A.Y.C.; Vemula, V., Facile fabrication of TiO_2-graphene nanocomposites (TGNCs) for the efficient photocatalytic oxidation of perfluorooctanoic acid (PFOA). J. Environ. Chem. Eng. **2018**, 6, 6359-6369. doi.org/10.1016/j.jece.2018.10.003.

50. He, D.; Li, Y.; Wang, J.; Yang, Y.; An, Q., Tunable nanostructure of TiO_2/reduced graphene oxide composite for high photocatalysis. Appl. Microsc. **2016**, 46, 37-44. doi.org/10.9729/AM.2016.46.1.37.
51. Had, O., Graphite and hexagonal boron-nitride have the Same Interlayer Distance. Why? J. Chem. Theory Comput. **2012**, 8, 1360-1369. doi.org/10.1021/ct200880m.
52. Dai, S.; Wu, Y.; Sakai, T.; Du, Z.; Sakai, H.; Abe, H., Preparation of highly crystalline TiO_2 nanostructures by acid-assisted hydrothermal treatment of hexagonal-structured nanocrystalline titania/cetyltrimethyammonium bromide nanoskeleton. Nanoscale Res. Lett. **2010**, 5, 1829-1835. doi.org/10.1007/s11671-010-9720-0.
53. Song, J.; Ling, Y.; Xie, Y.; Liu, L.; Zhu, H., One-pot engineering TiO_2/graphene interface for enhanced adsorption and photocatalytic degradation of multiple organics. Nanotechnology **2018**, 29, 395701. doi.org/10.1088/1361-6528/aacc56.
54. Zhang, L.-W.; Fu, H.-B.; Zhu, Y.-F.; Efficient TiO_2 photocatalysts from surface hybridization of TiO_2 particles with graphite-like carbon. Adv. Funct. Mater. **2008**, 18, 2180-2189. doi.org/10.1002/adfm.200701478.
55. Fan, X.; Zheng, W.; Singh, D., Light scattering and surface plasmons on small spherical particles. Light Sci. Appl. **2014**, 3, e179. doi.org/10.1038/lsa.2014.60.

56. Dilokekunakul, W ; Klomkliang, N ; Phadungbut, P; Chaemchuen, S ; Supasitmongkol, S. Effects of functional group concentration, type, and configuration on their saturation of methanol adsorption on functionalized graphite. Appl. Surf. Sci. **2020**, 501, 144121. doi.org/10.1016/j.apsusc.2019.144121.

57. Gao, W.Y.; Wang, M.Q.; Ran, C.X.; Yao, X.; Yang, H.H.; Liu, J.; He, D.L.; Bai, J.B. One-pot synthesis of Ag/r-GO/TiO2 nanocomposites with high solar absorption and enhanced anti-recombination in photocatalytic applications. Nanoscale **2014**, 6, 5498–5508. doi. 10.1039/c3nr05466g.

58. Fan, W.; Lai, Q.; Zhang, Q.; Wang, Y., Nanocomposites of TiO_2 and reduced graphene oxide as efficient photocatalysts for hydrogen evolution. J. Phys. Chem. C **2011**, 115, 10694-10701. doi.org/10.1021/jp2008804.
59. Xiang, Q.; Yu, J.; Jaroniec, M., Enhanced photocatalytic H_2-production activity of graphene-modified titanianosheets. Nanoscale **2011**, 3, 3670-3678. doi.org/10.1039/C1NR10610D.
60. Bahruji, H.; Bowker, M.; Davies, P.R.; Pedrono, F., New insights into the mechanism of

photocatalytic reforming on Pd/ TiO_2. Appl. Catal. B Environ. **2011**, 107, 205-209. doi.org/10.1016/j.apcatb.2011.07.015.

61. Rosseti, I., Hydrogen production by photoreforming of renewable substrates. ISRN Chem. Eng. **2012**, 2012, 964936. doi.org/10.5402/2012/964936.

62. Chiarello, G.L.; Ferri, D.; Selli, E., Effect of the CH_3OH/H_2O ratio on the mechanism of the gas-phase photocatalytic reforming of methanol on noble metal-modified TiO_2. J. Catal. **2011**, 280, 168-177. doi.org/10.1016/j.jcat.2011.03.013.

63. Chen, T.; Feng, Z.; Wu, G.; Shi, J.; Ma, G.; Ying, P.; Li, C., Mechanistic studies of photocatalytic reaction of methanol for hydrogen production on Pt/ TiO_2 by in situ fourier transform IR and time-resolved IR spectroscopy. J. Phys. Chem. C. **2007**, 111, 8005-8014. doi.org/10.1021/jp071022b

64. Bowker, M.; Gilbert, L.; Counsell, J.; Morgan, C., Dehydrogenation versus decarbonylation of oxygenates on Pd(110): pure, clean Pd is a Poor Catalyst. J. Phys. Chem. C **2010**, 114, 17142-17147. doi.org/10.1021/jp104837t.

65. Joo, J.B.; Dillon, R.; Lee, I.; Yin, Y.; Bardeen, C.J.; Zaera, F., Promotion of atomic hydrogen recombination as an alternative to electron trapping for the role of metals in the photocatalytic production of H_2. Proc. Natl. Acad. Sci. USA **2014**, 111, 7942-7947. doi.org/10.1073/pnas.1405365111.

66. Christoforidis, K.C.; Fornasiero, P., Photocatalytic hydrogen production: a rift into the future energy supply, ChemCatChem **2017**, 9, 1523-1544. doi.org/10.1002/cctc.201601659.

TOC/Abstract Graphic

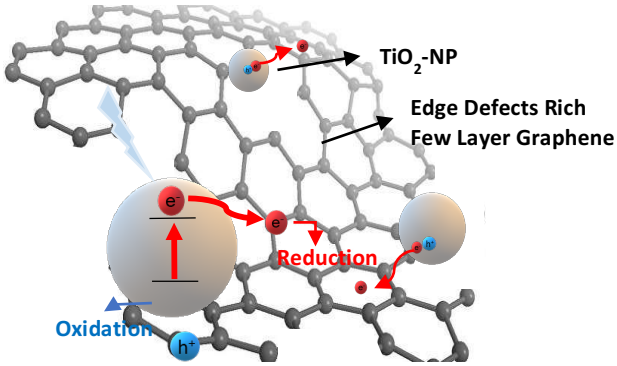

Synopsis

Few layer graphene obtained in rapid and eco-friendly exfoliation (in water) makes performant photocatalytic composite with TiO_2 for production of green energy (hydrogen).